BAV MAGAZINE
SPECTROSCOPY

## EDITORIAL

From the stars we basically receive only their electromagnetic radiation of different wavelengths, and we "see" essentially only the surface of the radiating bodies. By evaluating the light, we obtain information about:

- the direction of the radiation (positions and movement of the stars)
- the quantity of the radiation (brightness)
- the quality of the radiation (color, spectrum, polarization)

For amateurs, only the narrow band of visible light is easily accessible. In this spectral region, however, both the brightness (photometry) and the spectra of the objects can be examined. Today's amateur astronomy, with its instrumental and computer-assisted equipment, enjoys observation possibilities that were reserved exclusively for professional astronomers until a few years ago.

Thanks to the development of CCD technology, the types of observational perspectives have become much more varied. For example, in the area of variable star observation, there are many new possibilities in addition to already existing approaches.

Professional variable star research employs techniques and observation methods to study the physics and atmospheres of the stars in a holistic manner, considering all aspects and occurrences. Thus, this means that the collected radiation must be understood as a complex storage medium of the physical processes on and in the observed star.

This is appropriate for the intensity of the light, as well as for its spectral composition. The linking of brightness measurements and spectroscopy, a matter of course in professional astronomy, reflects this connection.

Along with brightness changes that occur in variable stars (which can occur quite frequently) variable changes in the state of the stars also can take place and often are revealed in the corresponding spectrum.

Ernst Pollmann

# BAV MAGAZINE SPECTROSCOPY

**Imprint**
The BAV MAGAZINE SPECTROSCOPY appears half-yearly from June 2017. Responsibilty for publication: German Working Group for Variable Stars e.V. (BAV), Munsterdamm 90, 12169 Berlin

**Editorial**
Ernst Pollmann, 51375 Leverkusen, Emil-Nolde-Straße 12, ernst-pollmann@t-online.de
Lienhard Pagel, 18311, Klockenhagen Mecklenburger Str. 87, lienhard.pagel@t-online.de
Roland Bücke, 21035 Hamburg, Anna von Gierke Ring 147, rb@buecke.de
The authors are responsible for their contributions.
Coverpicture:
HRDT2 (Astronomy & Astrophysics Royal Observatory of Belgium)

**Content** **Page**

BAV MAGAZINE
SPECTROSCOPY

# Temperature changes of Rho Cassiopeia
## Low-resolution Spectroscopy combined with Photometry

Martin Sblewski, Strausberg, Germany, m8neptun@t-online.de

**Abstract**

Rho Cassiopeiae (ϱCas) is a superlative example of a Yellow Hypergiant (YHG). It is a star with enormous luminosity, a radius that is one of the largest stellar radii of all, a mass about 40 times that of the Sun and, in addition, a pulsating variable of the semi-regular type. During a pulsation cycle, the spectral class can change from F8 to K0, encompassing more than one complete spectral class in the Morgan-Keenan (MK) system. The temperature, one of the main parameters of each star, changes with the spectral class and is thus subject to special interest when evaluating the observations.

ϱ Cas has been regularly observed by me photometrically and initially also spectroscopically since the beginning of 2017. This paper reports on the different approaches that have been used to try to detect a change in temperature spectroscopically, as well as to determine the absolute temperature photometrically using different approaches.

### Spectroscopic investigation

One of the main spectral features of the F-class is the G-band. The G-band is the CH molecule from 4299-4313Å with a total width of 14Å. Gray/Corbally [1] emphasizes its importance in spectral classification due to the rapid increase in intensity at low temperatures. Walker [2] refers to the G-band as the hallmark of the F-class and points out its relationship to the neighbouring H γ line.

The line ratio G-band/H γ is thus a reflection of the spectral class change and therefore also of the temperature change of a star. To theoretically reproduce this correlation, a synthetic spectra sequence was calculated from 5000K to 7000K with a stepping of 250K, as shown in Fig. 1. The software "Spectrum" used for this purpose was developed by Gray [3]. The parameters used for modelling, such as surface gravity, metallicity and microturbulence, correspond roughly to those of ϱ Cas. Since this is a qualitative estimate, thermodynamic atmospheric effects that the models cannot reproduce may be neglected.

In Fig. 1, the G-band is on the left, the FeI 4326Å line in the middle, and H γ on the right. The already mentioned increase in the intensity of the G-band towards low temperatures is clearly visible in the synthetic sequence. In an earlier project in May 2017, the Cepheid star δ Cephei was observed in a clear weather week continuously spectroscopically during a complete pulsation period (unpublished so far). The period of δ Cep is about 5.3 days.

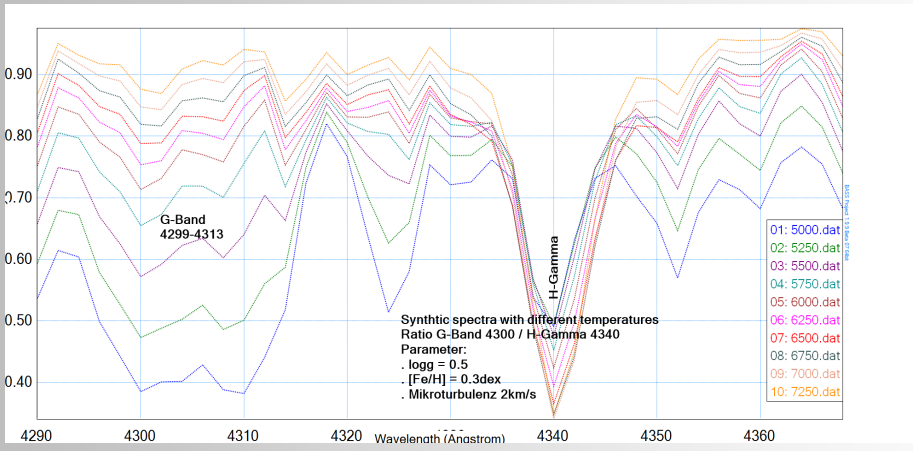


**Fig. 1**: Synthetic spectra sequence, spectral resolution Δλ 3Å, dispersion 2Å/Pix

During this time, the spectral class changes from F5 to G2 and back to F5. The spectrograph used is homemade, the grating has 600 L/mm, is rotatably mounted and can be adjusted in wavelength via a worm gear. The observed spectra of δ Cep were recorded slitless. The camera used was an Atik 314 L+ CCD camera. The dispersion is 1Å/pixel at an average resolution of R=500; the resulting signal-to-noise ratio is approximately 100. The spectra were processed with the software ESO-Midas [4].

Since δ Cep has already been continuously observed by me photometrically with a digital single-lens reflex camera (DSLR) over a longer period of time, photometric observations as well as spectroscopic ones were now available for analysis.

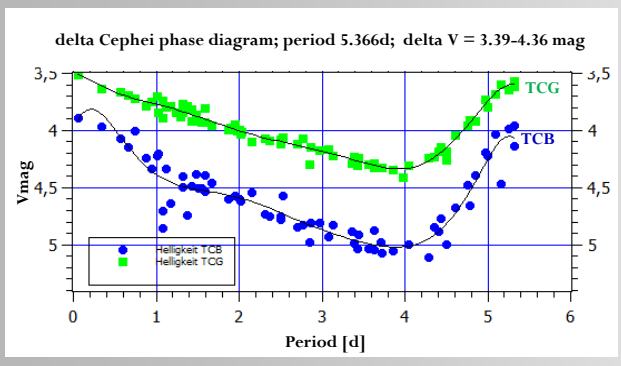


**Fig. 2:** DSLR observations

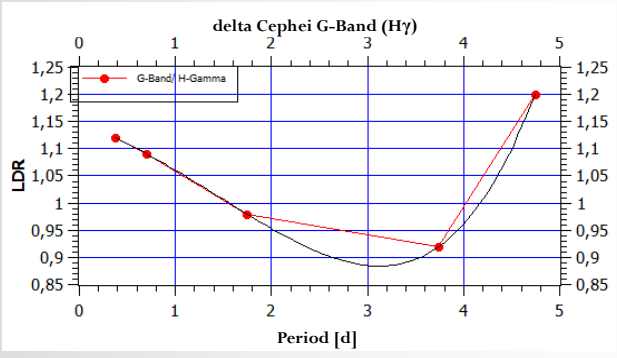


**Fig. 3:** LDR measurements

Fig. 2 shows the photometric measurements of the green channel and the blue channel of the DSLR. The varying difference of both curves already shows the change of the colour index (FI), which is the difference between green and blue and thus the change of the spectral class.

which is the difference between green and blue and thus the change of the spectral class. With an increasing FI in the minimum, the star becomes redder and thus cooler and later in its spectral class. Fig. 3 shows the intensity ratio from line depth ratio (LDR) measurements of the G-band to H γ during the above-mentioned week in May 2017. Both curves show very good agreement. The slow descent and the steep ascent are characteristic for the star's pulsation cycle. The temperature change that should be detected was therefore demonstrated. This result formed the starting point for the question of whether the temperature change of ϱ Cas can also be measured via the ratio of the G-band to H γ.

**Equivalent widths, Line intensities**

The analysis of the recorded spectra was initially carried out with measurements of the equivalent widths. When measuring the equivalent widths, the dependence of the spectral resolution on the nightly seeing, caused by the slitless recording technique, results in the problem that the measuring range cannot be reproduced exactly from one recording to the next.

In addition, due to the low resolution, the individual lines are not always completely resolved and therefore other lines included in the measuring range are also measured. An especially good example of this is the G-band. In its vicinity we find the FeI line 4326Å (Fig. 1). In the low-resolution spectrum, this line is rarely separable from the G-band. This results in measurement widths for the G-band that can vary between 40 and 50Å and thus also contain the FeI line.

The resulting measurement errors were unsatisfactory in the long-term. Therefore, the line depth was used to determine the line depth ratio (LDR) of G-band and H γ. The absorption core of the blend is always found at the same wavelength and is therefore both easier and more reliable to use (Fig. 3). This method, however, is reserved for clearly defined lines. For lines that are only slightly separated from the continuum, the measurement of the equivalent width is preferable.

**Determination of the continuum**

The normalization of spectra of spectral type F to K as they can occur with ϱ Cas, is often difficult to perform by hand, since the determination of the continuum is always subject to personal and thus arbitrary judgement. This can result in continuum ranges that are evaluated differently from one recording to the next, which in turn influence the measurement quality.

To minimize this source of error, the function ***CONTINUUM/SPEC*** from Midas is used for normalization. Midas calculates a polynomial curve of the continuum from an algorithm-supported weighting of the line profiles, which can then be used for normalization.

**Observations and Investigations on ϱ Cas**

**Fig. 4** shows a sum spectrum from 3 individual exposures with 300 s integration time each, as it typically appears after extraction in Midas.

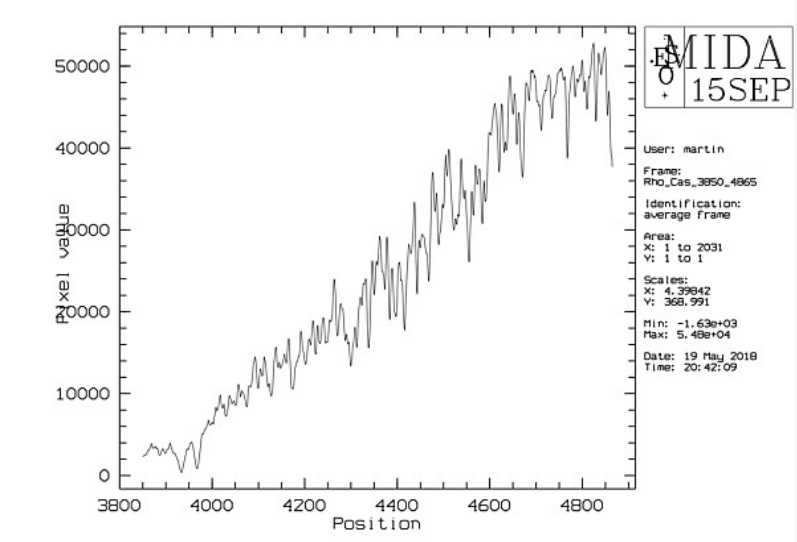


**Fig. 4:** Sum spectrum from 2018-05-12

Fig. 5 shows a representative selection of normalized spectra. The already described ratio of the G-band to H γ and the different quality of the resolution in the individual spectra are clearly visible.

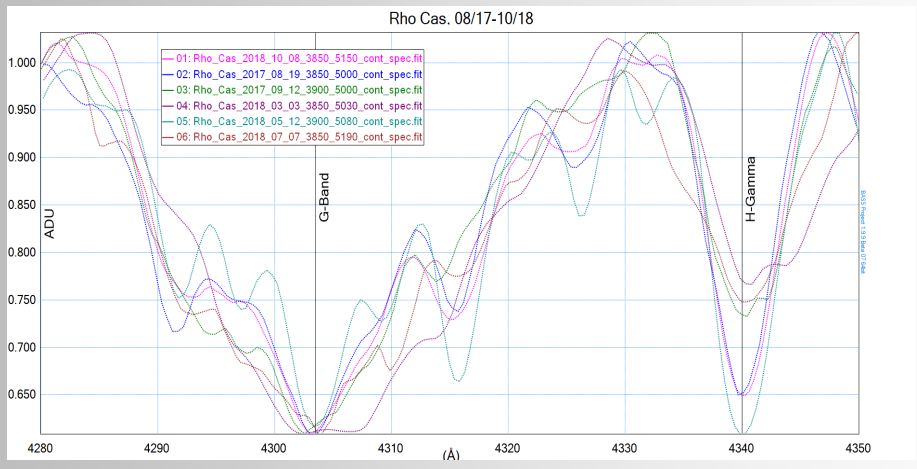


**Fig.5:** Selection of spectra from August 2017 to October 2018, wavelength range 4280-4350Å

**Fig. 6** shows the measurement of the LDR line ratio of the G-band to H γ for the period from March 2017 to October 2018. The black curve shows a 4th order polynomial that was placed over the measurement points to smooth the curve of the line ratio.

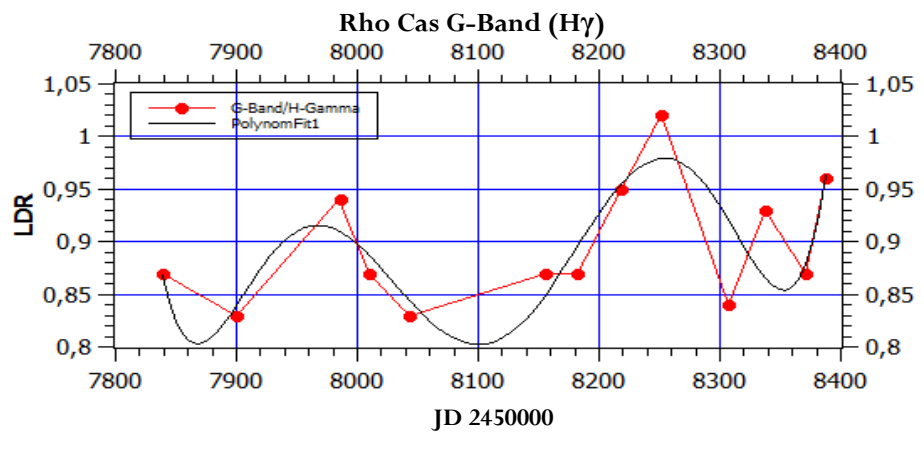


**Fig. 6:** Time behaviour of the line ratio based on the LDR line depth

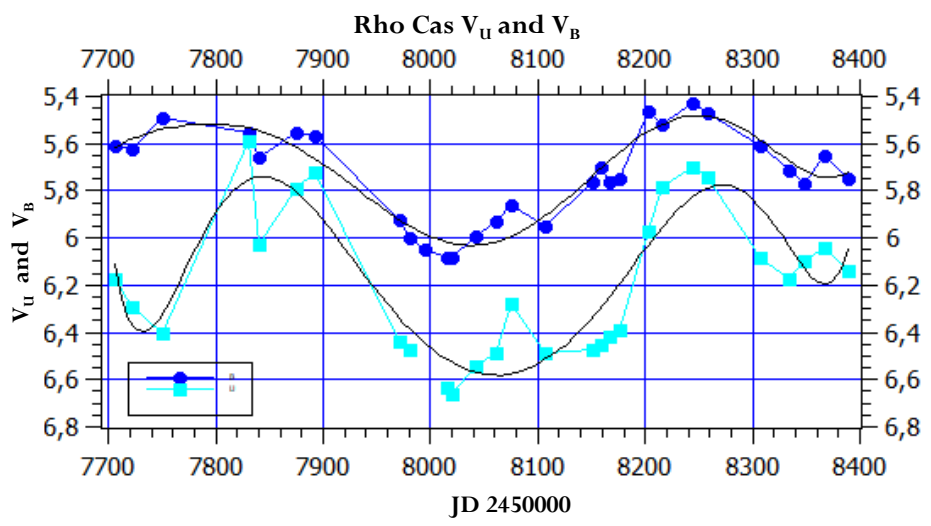


**Fig. 7:** Photometric light curves with Atik 383 L+ on TS Apo 60mm and Johnson-U/B filter of the same period as in Fig.6. The dark blue curve shows the B channel, the cyan curve shows the measured values of the U channel. Both curves were additionally provided with a polynomial as in Fig. 6, but with a 5th degree (black continuous line).

Fig. 7 shows my own light curves of the U- and B-channel for the observation period. Since the

early part of 2017, the photometric equipment has been complemented by a CCD camera and a photometric filter set in the Johnson UBVRI system. The filters U and B were selected for presentation because the amplitudes of the brightness changes are greatest here and they are therefore particularly well suited for visualisation. Even if spectroscopically and photometrically determined data do not coincide in every detail, a correlation of the polynomials in both data sets is clearly evident over time. From the photometric curve difference, the temperature change, as described above, is again qualitatively well recognizable.

The curve of the line ratio in Fig. 6 can also be understood as temperature variability. I.e., Fig. 6 and Fig. 7 each qualitatively depict the temperature variation with the change of spectral class or with the photometric brightness. However, an absolute determination of the photospheric temperature is not possible with this method. This is discussed in more detail in sections 2 and 3 of the article.

An attempt was also made to verify the temperatures derived from the individual spectra by means of flux calibration and Planck curve fitting at the maximum line flux. Nevertheless, the results were subject to such great fluctuations that this approach was abandoned thereafter. Also an attempt was made to create a thermometer for the LDR from G-band to H γ using known temperatures of standard stars [5]. Unfortunately, this attempt failed due to the low spectral resolution and the quality of the spectral images.

**Photometric investigations ofV-brightness**

Lobel et.al. [6] investigated in their paper the relationship between the V-brightness of ϱ Cas and the equivalent width of the FeI 5572Å line. This line is particularly well suited because it is not subject to any blends and is not disturbed by other spectral lines that could interfere with the cyclic behaviour which is correlated with the V-brightness.

From the measurements of the V-brightnes and the equivalent widths, they derived a linear progression and a formula for determining the surface temperature of ϱ Cas in the period of normal pulsations. The starting points are two spectra from 1993 and 1995 with temperatures of 7250 +/- 200K and 6500 +/-200K, respectively. Temperatures were determined from the measurement of 23 FeI and 11 FeII lines. To determine the equivalent widths and for comparison with the light curve, 78 spectra from the period from 1993 to 2002 were measured.

Quote Lobel: „On the other hand, the strong correlation of the Fe I line with V during the quiescent pulsation phases enables us instead to directly estimate Teff from V, by inserting equation (1) into equation (2): $T_{eff} = 9115 - 2525(V - 3.75)$ K “.

While the FeI 5572Å line is correlated with the brightness, the FeII lines behave anti-cyclically. The FeI 5572Å line showed an especially good agreement and was therefore used to create a linear function. The linearity is no longer given during the eruption phase, so that the formula can no longer be used to determine the temperature.

Similarly, low horizon heights during observation in summer, for example, can falsify the measurements and thus the result. The above mentioned uncertainties of the temperature determinations suggest that this is rather a rough temperature estimation and that no exactly calibrated temperature curve can be expected.

Figure 8 shows my photometric measurements in the Johnson-V channel converted to temperature in Kelvin. The shape of the curve is of course identical to that of the light curve, except that the ordinate now forms the temperature scale.

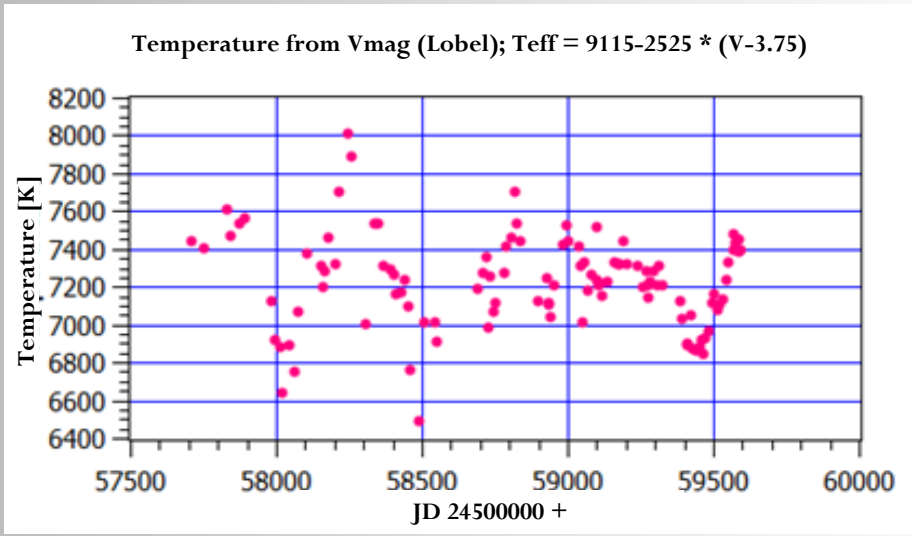


**Fig. 8:** Temperature curve from converted V-brightness from March 2017 to January 2022

**Determination of temperature from colour indices (FI's) U-B and B-V**

The idea for this investigation was based on the paper by van Genderen et.al. 2019 [7], in which photometric properties of ϱ Cas, V509 Cas and two other YHGs were studied. In the analysis presented here, an attempt was made to adopt the approaches of van Genderen et al. including the reported extinction and to make a comparison between the methods of Schmidt-Kaler (SK) and de Jager/ Nieuwenhuijzen (dJN). Thermometers were created for both methods and for both FIs (U-B and B-V), on which the temperatures from the own measurements will later be determined.

Method SK, calibration of the two FI's by means of polynomial fit to the data sets of SK [8] and Allen [9]. Spectral classes and temperatures are given by Allen for Ia, Iab, Ib Supergiants, while SK for Ia Supergiants gives values for U-B and B-V, see Tab. 1.

| Spektraltyp | B-V SK | U-B SK | Temperature [K] |
|---|---|---|---|
| A0 | 0.02 | -0.44 | 9980 |
| A2 | 0.03 | -0.3 | 9380 |
| A5 | 0.09 | -0.1 | 8610 |
| F0 | 0.17 | 0.15 | 7460 |
| F2 | 0.22 | 0.18 | 7030 |
| F5 | 0.31 | 0.27 | 6370 |
| F8 | 0.56 | 0.43 | 5750 |
| G0 | 0.75 | 0.52 | 5370 |
| G2 | 0.87 | 0.65 | 5190 |
| G5 | 1.03 | 0.82 | 4930 |
| G8 | 1.17 | 1.08 | 4700 |
| K0 | 1.25 | 1.18 | 4550 |
| K2 | 1.36 | 1.32 | 4310 |
| K5 | 1.6 | 1.8 | 3990 |
| M0 | 1.67 | 1.9 | 3620 |
| M2 | 1.71 | 1.95 | 3370 |

**Tab. 1:** Data set for the determination of a thermometer

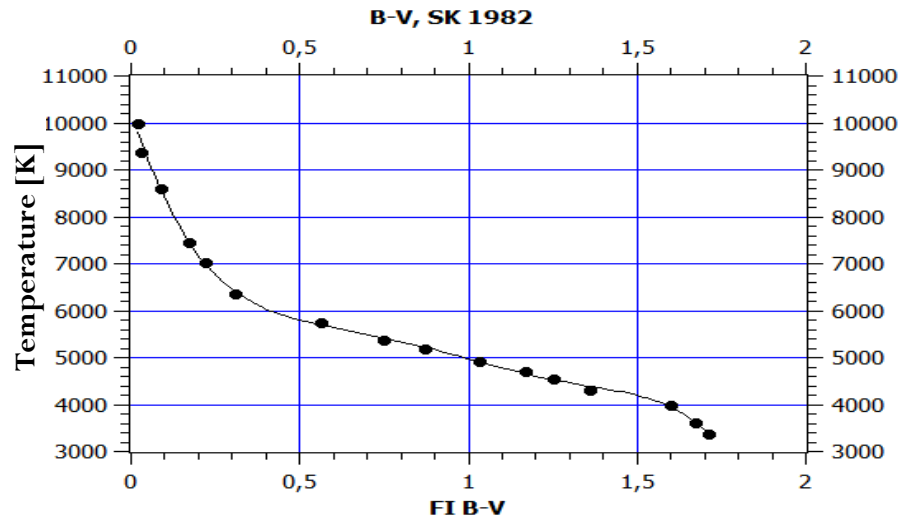


**Fig. 9:** Fit of the data set (Tab. 1) of SK FI B-V/Temperature

With the help of this data set, a polynomial was calculated, which can now be used to convert the self-measured FI's into a temperature value. Values above 10,000 K were excluded as they are not of interest for ϱ Cas and the curve can be fitted more easily (Fig. 9).This fit was also created for U-B, here the values are slightly more scattered; an error calculation results in a standard deviation of 78K for B-V and 122K for U-B.

**Method dJN, calibration of a temperature curve based on the luminosities and temperatures given by de Jager/Nieuwenhuijzen (dJN)**

C. de Jager and H. Nieuwenhuijzen [10] have published a paper in 1987 on the analysis of a data set with 199 observations on stellar bolometric luminosities and 268 observations on stellar temperatures. From this, they created a table giving the spectral classes, the luminosity classes and the corresponding temperatures. From these values on the hypergiants of the spectral classes from O5 to M4, luminosity class Ia+, thermometers were also developed and compared to the Allen/Schmidt-Kaler thermometers.

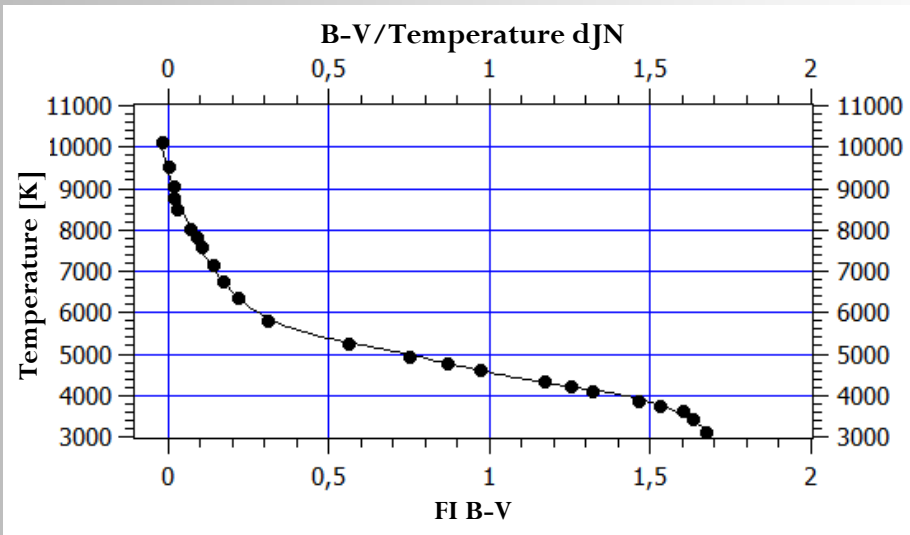


**Fig. 10:** Fit of the data set of dJN FI B-V/temperature

With the polynomials developed in this way, my own measurements could now be converted into temperatures. Figure 11 shows the comparison of the temperature curves for both methods for the colour index B-V. Van Genderen et.al. [7] state that the extinction E(B-V) for ϱCas is 0.45 and E(U-B) is 0.44. My own measurements were corrected for these values in order to achieve comparability with the results of van Genderen et al. [7].

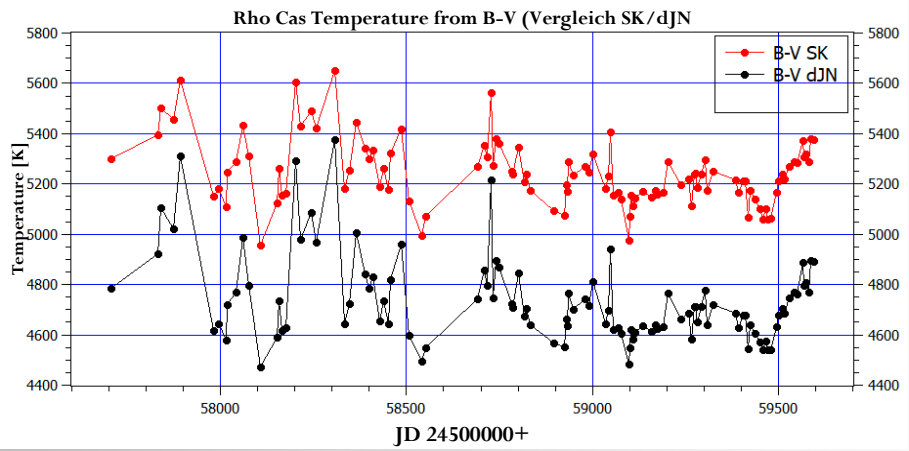


**Fig. 11:** Comparison of methods 1 and 2 for B-V with specification of temperature

The most striking feature of Fig. 11 is the height offset for both curves, B-V SK varies around a mean value of approx. 5200K, while B-V dJN is approx. 500K cooler at 4700K. Van Genderen et al. [7] refer to the lack of data for stars of luminosity class Iab for SK [8] 1982 and therefore recommend using the calibration of dJN [10] for stars of this class.

Van Genderen et.al. [7] compare photometric and spectroscopic data collected in 2010. With this they find the spectroscopic temperatures with approx. 1000K higher than the photometric temperatures of dJN [10]. The spectroscopic temperatures were found to be between 5777K and 6044K, while the photometric ones have varied between 4890K and 5040K.

The authors state that the reason for the difference is that the observed FI B-V is too red and an exact temperature determination is not possible photometrically. In the atmosphere of ϱ Cas, a high opacity layer is assumed to influence the photometric measurements. Rising stellar temperatures increase the mass loss and feed the high opacity layer, which in turn becomes more opaque. The absorptions of the photometric filters B and V do not change in a uniform way and therefore lead to an error in the colour index. This error increases towards higher temperatures and decreases significantly towards lower temperatures.

It should be noted that the temperatures determined in section 2 according to Lobel 2003 [6], which were obtained in connection with a spectroscopic basis and the photometric observations based on it, are significantly higher than those determined by van Genderen et.al [7] in the period of 2010. However, it is assumed that ϱ Cas was significantly hotter during the period of the underlying data from Lobel 2003 [6]. From my point of view as an observer, it should be noted that each FI consists of two individual measurements, which are subject to different error sizes

from one recording to the next. Consequently, error variables are included in the FI, which in the ideal case can cancel each other out, but in the worst case can also amplify each other to the maximum. With reference to my own measurements, this can be as much as 0.05 to 0.07mag in individual cases in B-V and under poor recording conditions, and as much as 0.1mag in U-B, leading to significant outliers in the temperature curve. For the purpose of completeness, the temperature determination from the FI U-B is shown in Fig. 12. Surprisingly, the curve based on dJN [10] fits much better to the temperature range given by van Genderen et.al. [7]. As this colour index is not investigated by the authors, no explanation can be given at the moment.

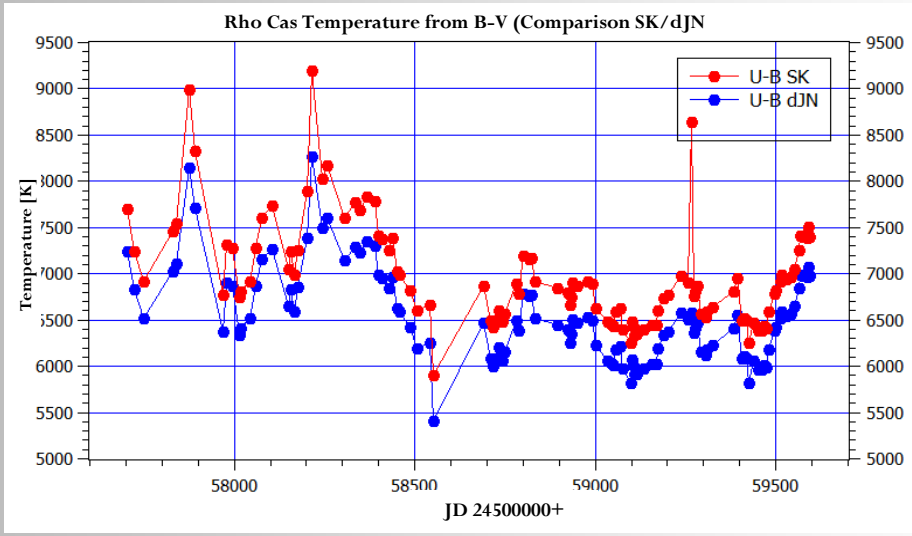


**Fig. 12:** Comparison of methods 1 and 2 for U-B

**Summary, conclusions, outlook**

It could be shown that temperature changes at ϱ Cas can be recorded with different observation methods. For the spectroscopic observations, it could be demonstrated that it is possible to assign changing temperatures with the help of the ratio of G-band to H γ. Nevertheless, it must be noted that the quality and resolution of the spectral images have a considerable influence on the quality of the results. Furthermore, it was not possible to determine the absolute temperature, but only to observe the temperature change. This remains reserved for high-resolution spectroscopy using recommended line ratios.

The project of low-resolution spectroscopy to observe the ratio of G-band to H γ was therefore already abandoned at the end of 2018 and only discussed again in the context of this article. The determination of temperature from photometric measurements using a colour

index is subject to variable influences of the stellar atmosphere that falsify the results and can therefore not be recommended. Further observation of FI U-B may be of interest if spectroscopically determined comparison temperatures are available. The most reasonable approach seems to be a further recording of the temperature from the measured brightness in the Johnson V channel, of course taking into account the limitations already mentioned in part 2. Although this curve follows naturally from a transformation of the brightness into a temperature range and not from the spectroscopically determined temperature, it can at least serve as an estimate of the current temperature conditions.

In the future, photometric data will continue to be recorded regularly and submitted to the AAVSO database, where they will be accessible to all interested astronomers. Many observing astronomers are hoping that ϱ Cas will be subject to another eruption in the near future. It would also be a special pleasure for me to be able to document such an event with my photometric measurements. For those who would like to know more precisely in which time periods outbreaks are to be expected, I recommend the recently published paper by G. Maravelias et.al. [11].

**References**

[1] 2008, R.O. Gray und C. J. Corbally, Stellar Spectral Classification

[2] 2013, R. Walker, Ein Führer durch die stellaren Spektralklassen

[3] R.O. Gray, https://www.appstate.edu/~grayro/spectrum/spectrum.html

[4] ESO-Midas, https://www.eso.org/sci/software/esomidas/

[5] 2006, Kovtyukh, High-precision effective temperatures of 161 FGK supergiants from line-depth ratios

[6] 2003, A. Lobel et.al., High-resolution spectroscopy of the yellow hypergiant ϱ Cassiopeiae from 1993 through the outburst of 2000-2001

[7] 2019, v. Genderen et.al., Pulsations, eruptions, and evolution of four yellow hypergiants

[8] 1982, Schmidt-Kaler, Calibration of special luminosity criteria b, Mv

[9] Allen, S-K 1982, Straizys, Calibration of MK spectral types including Teff and BC for main sequence, giants, supergiants

[10] 1987, C. de Jager and H. Nieuwenhuijzen, A new determination of the statistical relations between stellar spectral and luminosity classes and stellar effective temperature and luminosity.

[11] 2021, Grigoris Maravelias and Michaela Kraus, Bouncing against the Yellow Void - exploring the outbursts of ϱ Cas from visual observations

# Spectropolarimetry- or how to observe the magnetic field of a star with a telescope 72mm and a 3D printed spectrograph

Guillaume Bertrand, Nantes
gbe.astro@pm.me

**Abstract**

This study demonstrates that it is possible to detect and study the magnetic fields of a star with a 0.072m refractor, a polarimeter designed from 3D cinema glasses and a spectrograph produced in 3D printing. The chosen target is α2 CVn, an Ap-type star (chemically peculiar) widely studied for its magnetic field and its variability. In order to obtain a complete coverage according to the phase, 10 nights of observations were necessary. The Star'Ex spectrograph equipped with a grating of 2400 lines per mm and a slit of 10µm coupled to a 72mm f/6 refractor delivers spectra with an average resolution of ≈ 25000. We will rely on the Zeeman effect and calculate the Stokes I and V profiles on the Hα line to extract the information that interests us.

## Introduction

In November 2018, I came away very impressed from a conference given by Christian Buil at the RCE (Paris). This conference was entitled “Spectrography: the new Horizons". I learned there, among other things, that spectropolarimetry was on the way to becoming accessible to amateurs and making it possible to measure and map the field magnetism of the stars. Fascinating field of investigation… but which seemed to me at the time far from my possibilities! Since then, the years have passed and the formidable Star'Ex spectrograph manufactured with a 3D printer has appeared, making it possible to make high resolution spectra of very good quality. In parallel, the field of possibilities with the Sol'Ex project (Star’Ex dedicated to the sun) has evolved and it is now possible to produce magnetograms using a polarimeter made from 3D cinema glasses.

I thought it would be great to adapt this little polarimeter for stars and to try to detect the polarization of the bright star α2 CVn (Cor Caroli) located about 110 light years from us. This is the first star classified with the type “Ap”, chemically particular, which has been the subject of many studies about its variability and its magnetic field. The challenge for me was to confirm the detection with a modest configuration, accessible to all: a 72mm SkyWatcher refractor f/6 on a HEQ5 mount associated with the Star'Ex spectrograph.

## Methodology

The measurement of the magnetic field of a star is made possible thanks to the Zeeman effect. This quantum effect shows that within a spectrum, certain "magneto-sensitive" lines will divide into several components in the presence of a magnetic field. These components are circularly polarized for the longitudinal field (in the line of sight) and linearly (perpendicular to the axis

sight) for the transverse field. The sensitivity of the line to the magnetic field is defined by the Landé factor between 0 and 3. To better represent the phenomenon here is a small video of the ESO proposing a visual representation of the Zeeman effect:

Zeeman Effect - Control light with magnetic fields - YouTube

The polarimeter built for the Sol'Ex allows us to isolate the polarization circular left (-45°) and right (+45°). It allows us to measure the longitudinal magnetic field.

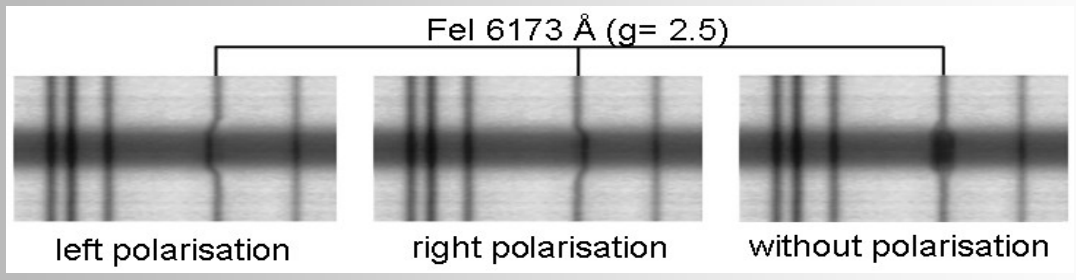


**Fig. 1:** Simulation of a solar spectrum with a passing sunspot. The Fe I line is deformed by the the magnetic field of the spot. The polarimeter allows to isolate left and right polarization. To give an order of magnitude : a longitudinal mean field of 1000 Gauss distorts the line by 0.0445 Å.

**Fig. 2:** The two "left" and "right" filters of the polarimeter made with 3D cinema glasses. Each "glass" (plastic) consists of a polarizing plate and a quarter-wave plate at -45° or + 45° depending on the eye

**Observation strategy**

Observation strategy: The acquisitions are carried out in sequence in an accurate order. Note that the exposure time (1h47 per night) is quite substantial for a target of magnitude 2.81. In question are the "homemade" polarimeter which leads to a loss of flow (40% less flow) which is not negligible and the small diameter of the instrument (SW72ED refractor f/6).

Spectropolarimetry or how to observe the magnetic field of a star

***Acquisition sequence:***
$I_L$ (λ) 2 x 800s (polarization left)
$I_R$ (λ) 2 x 800s (polarization right)
$I'_R$ (λ) 2 x 800s (polarization right)
$I'_L$ (λ) 2 x 800s (polarization left)

The Stokes parameters I and V corresponding respectively to the total intensity measured (strictly positive) and at the rate of circular polarization, which can be positive or negative depending on the direction of rotation are calculated using the relationship next:

$$\frac{V(\lambda)}{I(\lambda)} = \frac{[I_L(\lambda) - I_R(\lambda)] + [I'_L(\lambda) - I'_R(\lambda)]}{I_L(\lambda) + I_R(\lambda) + I'_L(\lambda) + I'_R(\lambda)} \qquad (1)$$

The null-polarization spectrum allowing the measurement error to be estimated is obtained with the relationship:

$$\frac{N(\lambda)}{I(\lambda)} = \frac{[I_L(\lambda) - I'_L(\lambda)] + [I_R(\lambda) - I'_R(\lambda)]}{I_L(\lambda) + I_R(\lambda) + I'_L(\lambda) + I'_R(\lambda)} \qquad (2)$$

The ephemeris adopted for the phase calculation is the following (Farnsworth, G. 1932, ApJ, 75, 364):

$$JD = 2419869.720 + 5.46939 \cdot E \qquad (3)$$

The easiest data to obtain from the previously calculated data is the longitudinal field $\boldsymbol{B_l}$ expressed in gauss - i.e. the component of the magnetic field in the line of sight - which is related to the Stokes parameters ***I*** and ***V*** to through the following equation (Donati et al, MNRAS 291, 658-682, 1997):

$$B_\ell(G) = -2.14 \times 10^{11} \frac{\int vV(v)dv}{\lambda_0 g_{eff} c \int [Ic - I(v)]dv} \qquad (4)$$

where ***Ic*** is the unpolarized continuum, *v* is the radial velocity, c is the velocity of the light in the same unit as *v*, $\lambda 0$ is the central wavelength of the line in nm, and $g$ is the effective Landé factor of the line.

**Simulations**

Here are two simulations to better represent the measured phenomenon:

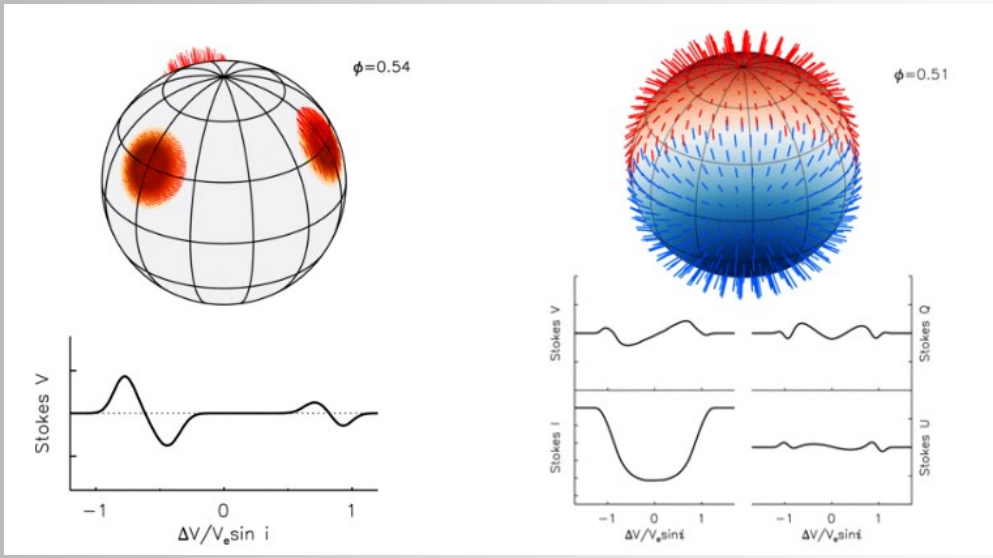


**Fig. 3:** Late-type active stars have small-scale structured magnetic fields. They can be detected and characterized using high resolution spectroscopy combined with circular polarization analysis. The Stokes V signatures of the magnetic spots move along the profile of the line and change shape and amplitude as function of the orientation of the field inside the spot. Source: Oleg Kochukhov.




**Fig. 4:** Some early-type stars exhibit very strong and generally organized magnetic fields. Their magnetic geometries can be described approximately with a dipole inclined with respect to the stellar axis of rotation. For such stars, we can measure and interpret the variation of the profile of the line in the four Stokes parameters. Stokes V spectra provide information on the magnetic component of the line of sight while the linear polarization spectra (Stokes Q and U) characterize the transverse magnetic field. Source: Oleg Kochukhov

**Observations and treatment**

The sightings (eleven nights) were spread between June 30, 2022 and July 15, 2022 with the equipment described below. “Observatory” located in La Montagne (44) near the city of Nantes.

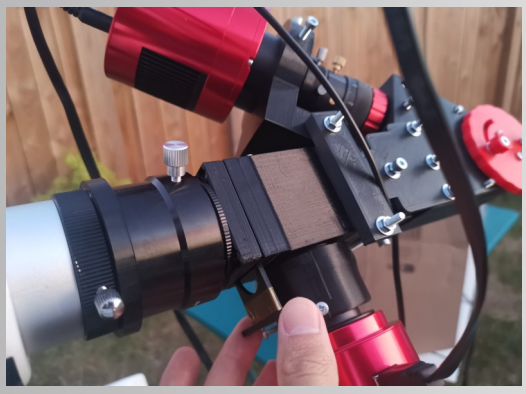

**Fig.5:** The polarimeter is placed in front of the spectro guide cube. Closer to the slot would have been better to limit the optical defects of the flexible lenses of the glasses but I wanted to make it as simple as possible in terms of assembly.

**Fig.6:** SkyWatcher 72ED f/6 refractor; Star'Ex 2400 L/mm spectrograph, 80x125, 10 µm slit. Polarimeter 3D cinema glasses ux1rgkgdauY); Science camera: ASI 183 MM PRO; Guide camera: ASI 178 MM; Mount: Heq5 Pro

## Results

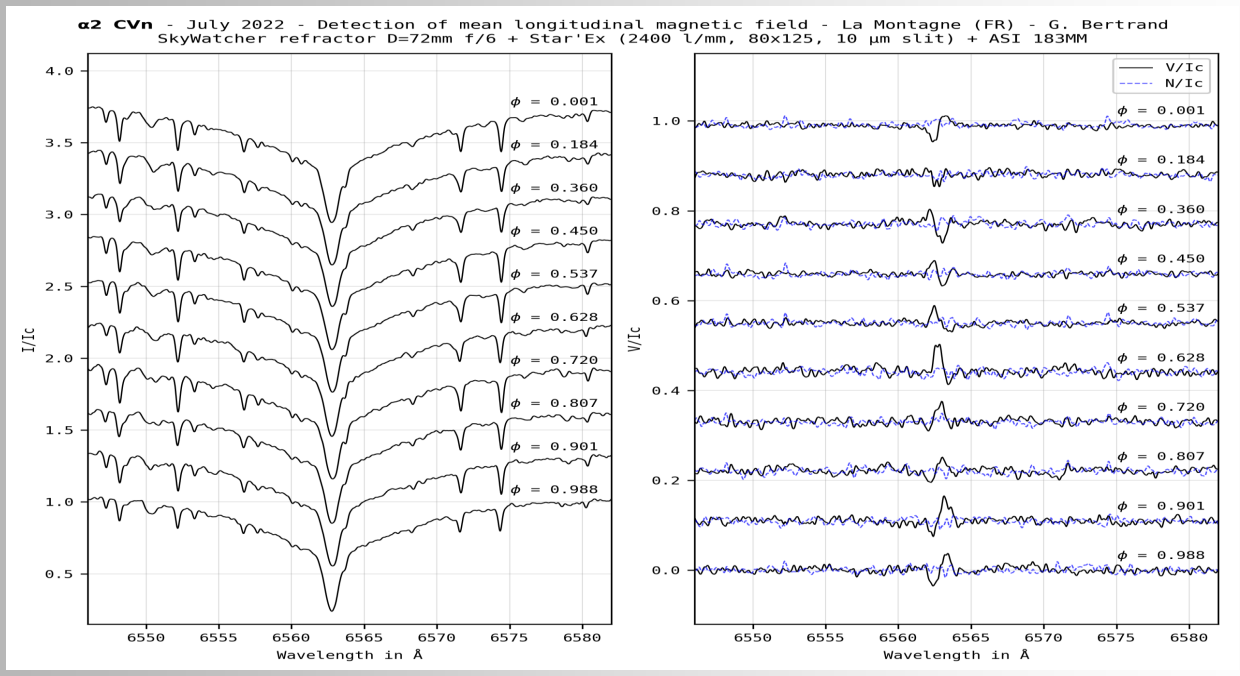


**Fig. 7:** α 2CVn magnetic field detection of July 2022

**Figure 7:** Left to right
I/Ic: Total intensity measured
V/Ic: Circular polarization rate
N/Ic: Spectrum at zero polarization used to estimate the measurement error.

Spectra acquisition is performed with SharpCap and PHD2. Pre-processing is done with specINTI. The calibration is carried out in lateral mode (4 optical fibers at the telescope input) with a neon bulb. The average resolution of observations with the configuration is about 25000 and the signal to noise ratio is greater than or equal to 150. A Python script has been developed to correct the heliocentric velocity spectra, normalize the continuum, calculate the Stokes parameters I and V and present the results in the form of graphics.

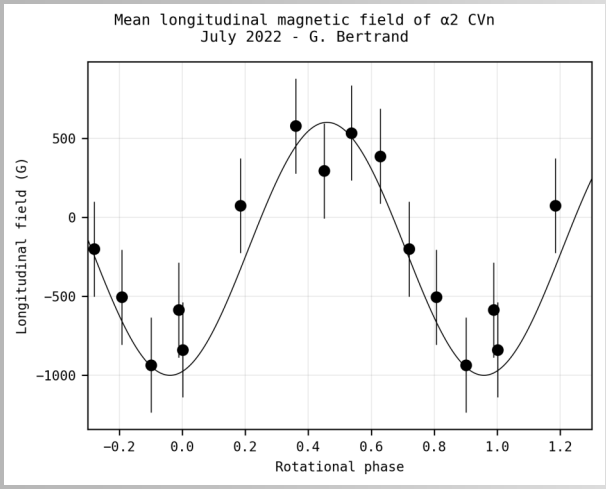


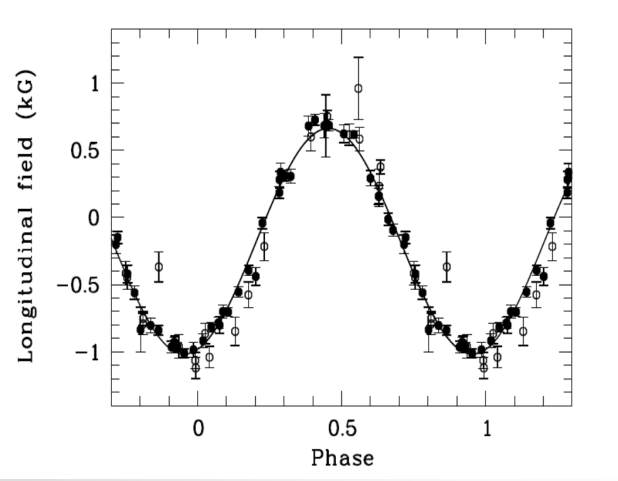


**Fig. 8:** Mean longitudinal magnetic field calculated for the Hα line from equation (4). Error bars are calculated from the delta between the two points of measurement close to phase 0.

**Fig. 9:** To compare with Fig. 8 here are results from D. Monin et al. on the Hβ line: arXiv:1203.0278 (2012)

A circular polarization signal is detected at the level of the Hα line on the V component of the Stokes parameter (Fig. 7, middle plot). The signal to noise ratio is not excellent but the result is reinforced by the zero polarization spectrum which does not indicate strong measurement bias. Moreover, there is a clear correlation between these results and the results of O. Kochukhov et al. (A&A 513, A13, 2010) and C. Buil. The polarization rate pattern is repeated periodically depending on the phase putting highlight the rotation cycle of the star (P = 5.47 days). It is from

these elements that professional astronomers study the mechanisms of stellar magnetism and reconstruct maps of the magnetic field and the surface of stars. The capabilities of this small 3D printed Star'Ex spectrograph coupled with the small SW72ED refractor are really stunning! The result is beyond my expectations. This is beautiful astrophysics at the limit of instrumentation but in truth quite easily accessible with a bit of method.

**Next step…reconstruct an image of the star's surface**

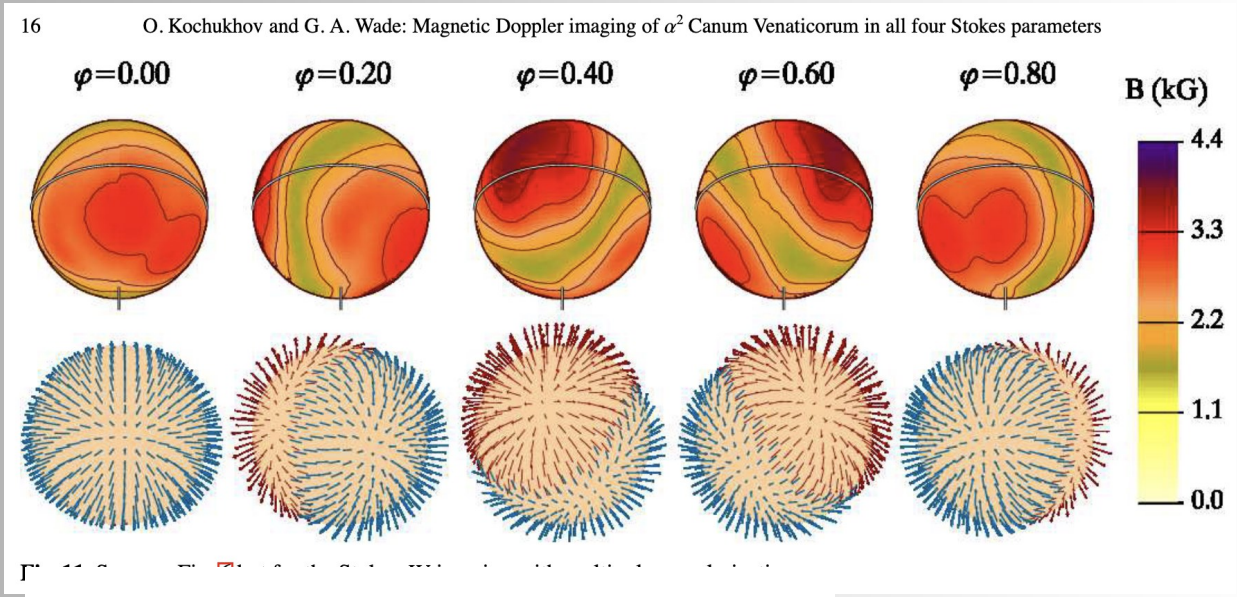


**Fig. 10:** Example of reconstruction of the Cor Caroli magnetic field using parameters I and V of Stokes (taken fromO. Kochukhov et al. 2010)

Professionals use a complex technique to map the magnetic field and the distribution of elements on the surface of stars by inverting a high resolution spectrum time series. This technique is named ZDI for Zeeman Doppler Imaging. The periodic modulation of the Zeeman effect as a function of the rotation period of the star is used to iteratively reconstruct the distribution of the magnetic field at the surface of the star. This technique uses the principle of image reconstruction by entropy maximization; it generates the geometry of the magnetic field (see the technique spherical harmonics) by synthesizing the Stokes IV profiles to match the observations.

A prerequisite for the ZDI to work is that the width of the intrinsic line be lower than the broadening induced by the rotation of the star (Doppler effect). It's unfortunately not the case

for Balmer lines, including the Hα line. For this reason, these lines are less usable for Zeeman imaging than lines of heavier elements (in particular Fe II 4923, 5018, 5169 Å) that have a higher Landé factor, higher than the Hα line, therefore a more marked signature of the Stokes profile.

However for stars of type α2 CVn we can model their fields magnetic fields assuming oblique dipole geometries. Most ZDI studies find local deviations from these geometries, but confirm at the same time that the oblique dipoles provide a very good first approximation of stellar magnetic fields.

After long hours of research, I managed to get my hands on an algorithm Python allowing me to do "ZDI". It is written by C. P. Folsom (7) following the method from Donati et al. (8, 12). To date, I have developed a first Python script allowing me to prepare the spectra and to create the input files that the model will consume. The model is partly constrained using the fundamental parameters of the star, the rest of the parameters are free.

The idea is now to create a second script allowing me to play with these free parameters in order to make the model converge towards the best solution. It is the most sensitive stage… Indeed, depending on the parameters adopted, the results may differ altogether. ***Results to come…***

**Summary**

This study demonstrates that it is possible to detect and study the magnetic field of a star with a 0.072m bezel, a polarimeter designed from 3D cinema glasses and a spectrograph made in 3D printing. The chosen target is α2 CVn, a widely studied (chemically peculiar) Ap-type star for its magnetic field and its variability. In order to achieve complete coverage depending on the phase, 10 nights of observations were necessary.

The Star'Ex spectrograph equipped with a grating of 2400 lines/mm and of a 10µm slit coupled with a 72mm f/6 telescope delivers spectra with an average resolution of 25000. We will rely on the Zeeman effect and calculate the Stokes I and V profiles on the Hα line to extract the information that interests us.

**References**

[1] Magnetic Doppler imaging of α2 Canum Venaticorum in all four Stokes Parameters O. Kochukhov et al , A&A 513, A13 (2010)

[2] Stokes IQUV Magnetic Doppler Imaging of Ap stars II: Next Generation Magnetic Doppler Imaging of α2 CVn O. Kochukhov et al , arXiv:1402.2938v1 (2014)

[3] Doppler Imaging of stellar magnetic fields III. Abundance distribution and magnetic field geometry of α2 CVn O. Kochukhov et al , A&A 389, 420–438 (2002)

[4] Measuring magnetic fields of early-type stars with FORS1 at the VLT S. Bagnulo et al, A&A 389, 191–201 (2002)

[5] Doppler Imaging of stellar magnetic fields I. Techniques N. Piskunov and O. Kochukhov, A&A 381, 736-756 (2002)

[6] Doppler Imaging of stellar magnetic fields II. Numerical experiments O. Kochukhov et al, A&A 388, 868–888 (2002)

[7] The evolution of surface magnetic fields in young solar-type stars II: the early main sequence (250-650 Myr) C.P. Folsom et al, arXiv:1711.08636 (2017)

[8] Zeeman-Doppler imaging of active stars. II. Numerical simulation and first observational results. Donati, J. -F. et al, Astronomy and Astrophysics, Vol. 225, p. 467-478 (1989)

[9] Chaîne Youtube astro-spectro C. Buil, https://www.youtube.com/channel/UCdlVj1AAV7y_KxBIwhjChug

[10] Le projet Sol'Ex & Star'Ex C. Buil, www.astrosurf.com/solex/

[11] Magnetic field structure in single late-type giants: The weak G-band giant 37 Comae from 2008 to 2011, S. Tsvetkova et al, arXiv:1612.02669v1 (2016)

[12] Spectropolarimetric observations of active stars J.-F. Donati et al, Mon. Not. R. Astron. Soc. 291, 658-682 (1997)

[13] Zeeman Doppler imaging of active stars J.F. Donati and S.F. Brown, A&A (1997)

[14] Magnétométrie stellaire et Imagerie Zeeman-Doppler appliquées à la recherche d'exoplanètes par mesures vélocimétriques Elodie E. Hebrard, https://tel.archives-ouvertes.fr/tel-01309532

[15] High-precision magnetic field measurements of Ap and Bp stars
G. A. Wade et al, Mon. Not. R. Astron. Soc. 313, 851±867 (2000)

# Measuring the redshift of galaxy NGC7469 to determine the Hubble Constant

Melina Anna Mitsakos, excerpt of a work on the astronomy project course
at the CFG observatory, Wuppertal, Germany
melina-anna.mitsakos@sgw.logineo.de

## Abstract

The focus of my work presented here will be measuring the redshift of a galaxy that is moving away from us due to the expansion of the universe. If the redshift of a galaxy spectrum is determined, the radial velocity of the galaxy can be calculated. Knowing the distance and radial velocity of a distant object, the current Hubble constant $H_t$ can be approximated with the linear relationship $H_t = v_r(t)/r(t)$.

## Introduction

I chose the galaxy NGC7469 (Fig. 1) as the object for. This galaxy is a type SB(rs)a spiral galaxy with an active galactic nucleus (AGN) and is assigned to the Seyfert1 category. It has a visual magnitude of 12.09 and is located in the constellation Pegasus at 23h03m15.62s right ascension and +08°52'26.4" declination. The distance of NGC7469 was determined to be r = 56.29 Mpc (± 12.15) [1] . It is interesting that this galaxy was one of the first to be observed by the James Webb Space Telescope, although the picture has not been released yet (September 2022) [2]. Thus the following one is still from the Hubble Space Telescope.

**Fig. 1:** The Galaxy NGC 7469

## Instrumentation

To record the spectrum of the galaxy NGC 7469 (Fig. 1), the Schmidt-Cassegrain telescope C14 EdgeHD from Celestron was used on a 10Micron GM2000HPS mount (Fig. 2) in the private observatory of Bernd Koch (Sörth/Westerwald, Germany).

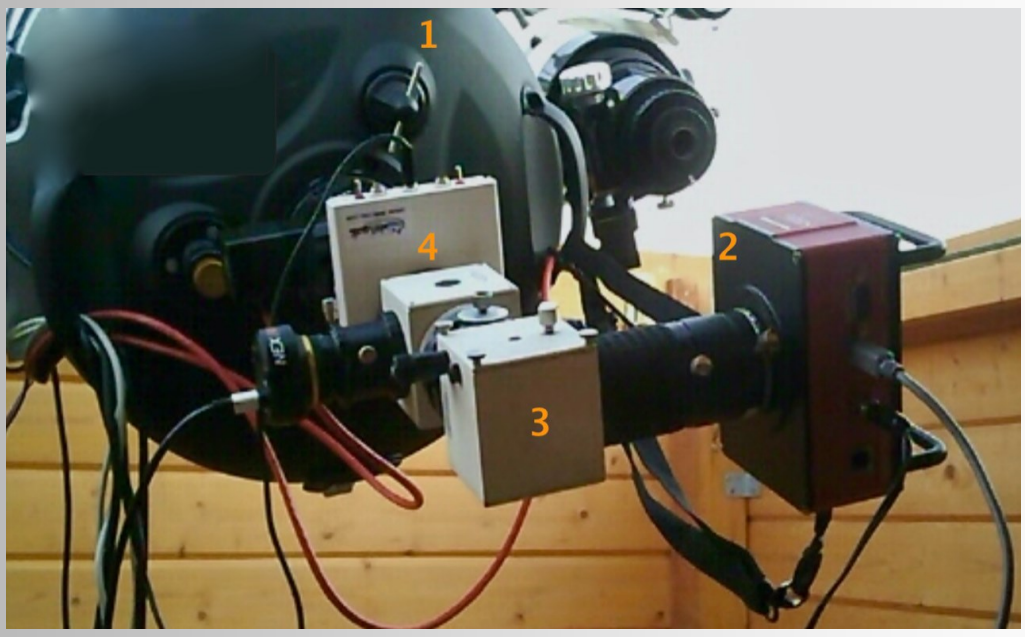


**Fig. 2:** The instrumentation:
Telescope (1), camera (2), spectrograph (3) and reference lamp (4)

The telescope has a maximum focal length of 3.81 m with an aperture of 0.356 m. The maximum aperture ratio is therefore f/10.8. When recording the spectra, a reducer was used, with which the focal length was reduced to 2.74 m and thus the aperture ratio was f/7.7. The SBIG STF-8300M was used as CCD camera and the DADOS slit spectrograph from "Baader Planetarium" (Germany) was used as spectrograph (Fig. 2).

The spectra were recorded using the 50 µm slit and a 300 lines/mm grating, which results in lower resolution, but is favorable used for faint objects such as distant galaxies in order to achieve an acceptable signal/noise ratio. The spectrum of the NeAr reference lamp PF0037-Alpy Calibration Module functioned as reference for the calibration of the galaxy spectrum.

**Observation**

Due to the good observation conditions in Sörth (Westerwald, Germany) and the favorable time, the spectra were recorded in the observatory of Bernd Koch (IAU station code: B72) via remote control as part of a video conference.

The telescope was aligned with the Stellarium software, while the camera was controlled with MaxIm DL Pro5. First, the time of the computer and the mount was synchronized and the DADOS was manually focused using the NeAr reference lamp. A total of 15 images, each with an exposure time of 300 s, and 10 darkframes, each with an exposure time of 300 s, were taken from the spectrum of the galaxy. For the flatframes, the camera was exposed to a bright LED screen 10 times for 300s.

Genarally, when taking pictures, it must be noted that the light paths are distorted by air currents in the atmosphere (astronomical seeing) and that the resulting erratic movement of objects requires precise tracking of the mount (guiding), and several individual pictures, so that the best of them can be selected and combined into one image (Lucky Imaging). Other difficulties are light pollution from surrounding light sources and atmospheric dispersion, which is why objects higher above the horizon are preferred. Atmospheric dispersion is a problem insofar as the light of the observed object is already split up into its spectral components in the air and therefore the light is no longer concentrated on the slit of the spectrograph, which is why part of the light and thus also part of the information is lost.

**Evaluation process**

The following steps to calibrate the raw images were carried out with MaxIM DL Pro5. First, all of the images in one category (i.e. bias, dark and flat) were stacked into a composite image, with an average value for each individual pixel being calculated from the intensities of the same pixel from all images. The MasterDark was then subtracted from the lightframe so that the noise is eliminated from the image.

As a result, the exposure time of the darkframes cannot be reduced too much because it has to be the same for the lights and darks. However, the noise in the images can be minimized by recording many darks and then averaging them, since the noise decreases with the square root of the number of recordings. The readout noise, also known as bias, is caused by the data transfer from the camera to the computer and occurs in all recordings, so it is eliminated by subtracting the MasterBias from the light.

Varying amounts of light automatically fall into different areas of the telescope due to its cylindrical opening, resulting in a darkening towards the edge (vignetting). In order to capture this vignetting and dirt on the camera or in the beam path, exposure is made against a bright surface. After the recording, the pixel brightness of the lightframe is divided by the MasterFlat. Since the vignetting and the dust grains are both in the lightframe as well as in the MasterFlat, this results in a pixel value of one.

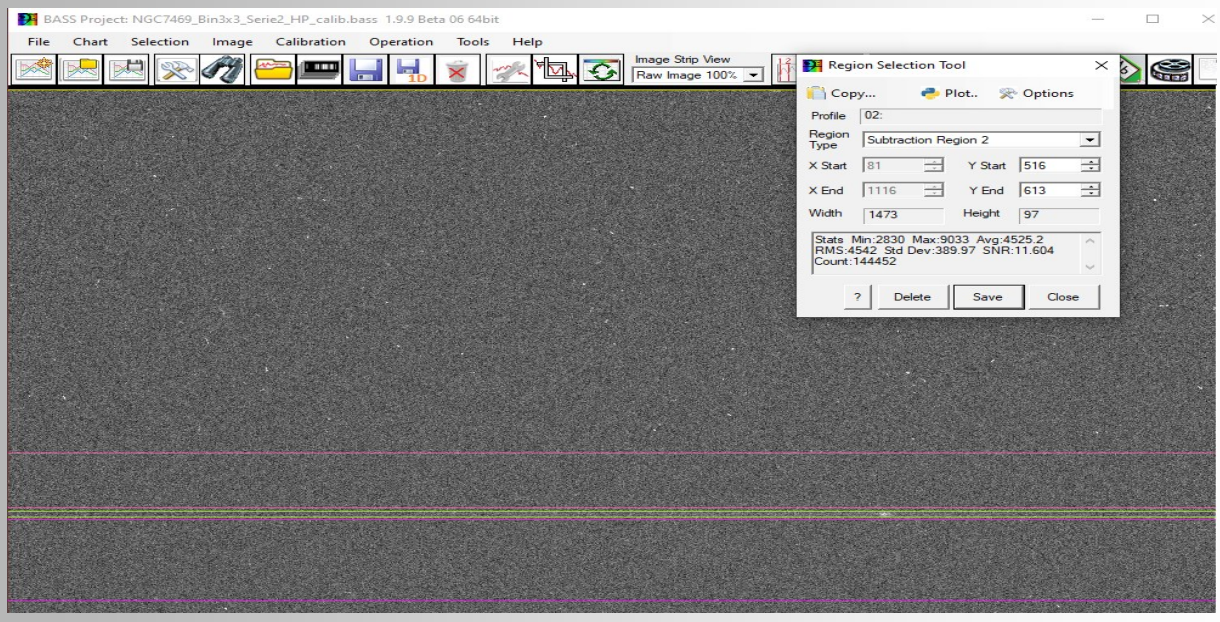


**Fig. 3:** Stack of 15 spectra, exposed 300s each. The scan of the Hα emission line will be carried out within the green lines. The sky and noise background to be subtracted is framed pruple.

Cosmics that only occur in the lightframe do not therefore disappear. Since the image has a "flat" background (without vignetting) after this processing step in regard to the brightness intensity, the final image is also called flat field. The following formula is used to eliminate errors using image mathematics:

Calibrated picture = (Lightframe-MasterDark)/(MasterFlat-MasterDark)

The processing steps mentioned were carried out automatically with MaxIM DL Pro5 with the "Batch Save and Convert (with Calibration)" function. Furthermore, those pixels that are hot and cold pixels were corrected in the calibrated image with the "Kernel Filters" and "Clone Tool" functions. The intensity values of the pixels from the immediate vicinity of the faulty pixel were taken, averaged and set as the new pixel intensity value.

Care must be taken not to falsify the spectrum. Therefore, nothing was changed in the area of the spectrum itself, only the environment was cleaned up. In order for an object to be recognizable, the signal/noise ratio should be larger than two. The stacked, calibrated and cleaned image is shown in Fig.3. The software BASS was used for further evaluation of the data.

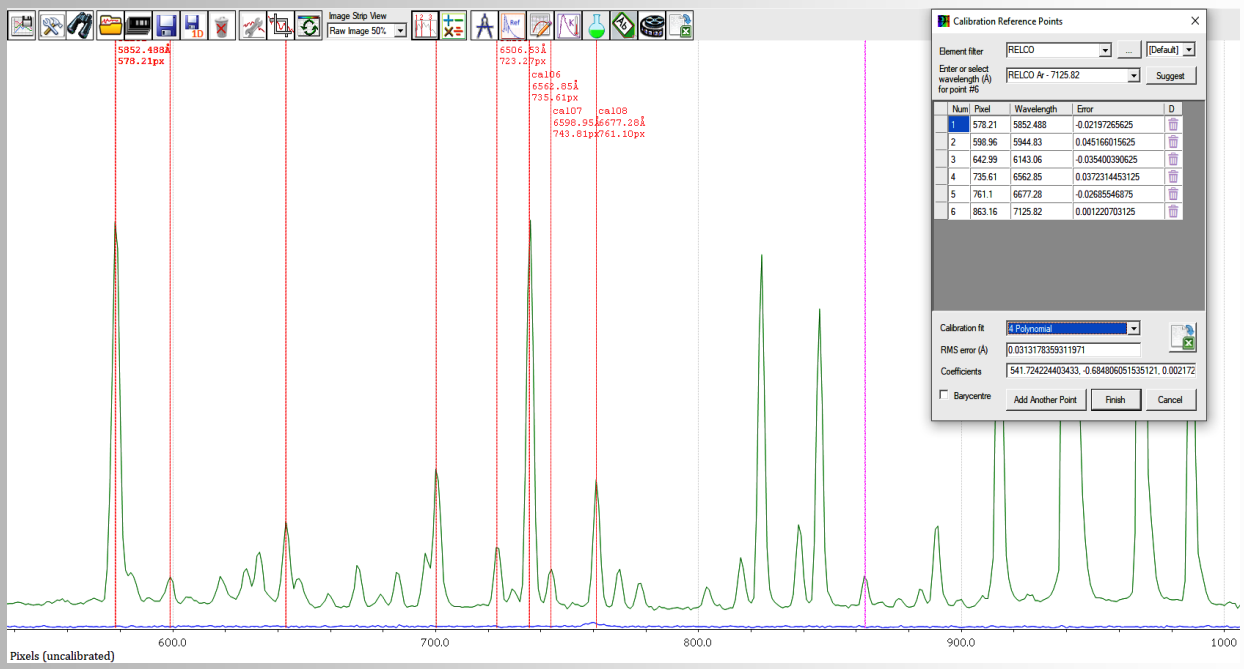


**Fig. 4**: Calibration of the NeAr reference spectrum with known emission lines

With BASS I analysed the emission spectrum of the NeAr reference lamp (green line) by enclosing six known peaks and assigning them the corresponding wavelengths (Fig. 4) [3]. After that, the galaxy spectrum (blue line) could be loaded, whereby the wavelength assignment based on the calibration coefficients of the NeAr reference spectrum in Fig. 4 was now specified. It became apparent that the emission lines of the galaxy spectrum were not in the expected wavelength ranges, but were clearly shifted to the right, which can be attributed to a strong redshift. Consequently, I determined the wavelength of the Hα line with several Gaussian fits in the intensity maximum (Fig. 5) and averaged the measured wavelengths. Using this average wavelength and the resting wavelength of the hydrogen line Hα of $\lambda_0 = 6562.852$ Å, the redshift z could be calculated as follows:

$$z = \Delta\lambda/\lambda_0 = (\lambda_{measured}/\lambda_0)\text{-}1 = (6670.741\text{Å}/6562.852\text{Å})\text{-}1 = 0.01644$$

In the spectrum processing program BASS, the NGC7469 spectrum could finally be corrected for the amount of the earth's rotation and the rotation of the earth around the sun. In addition, BASS allows the calculation of the speed at which NGC7469 is moving away from Earth. To emphasize the emission lines of the galaxy spectrum, it was normalized to a relative intensity of 1, for which purpose a largely peak-free section of the spectrum with low noise was selected (6400Å-6500Å). The fully calibrated spectrum of NGC7469 is shown in Fig. 6 in blue, as well as the redshift corrected spectrum in purple.

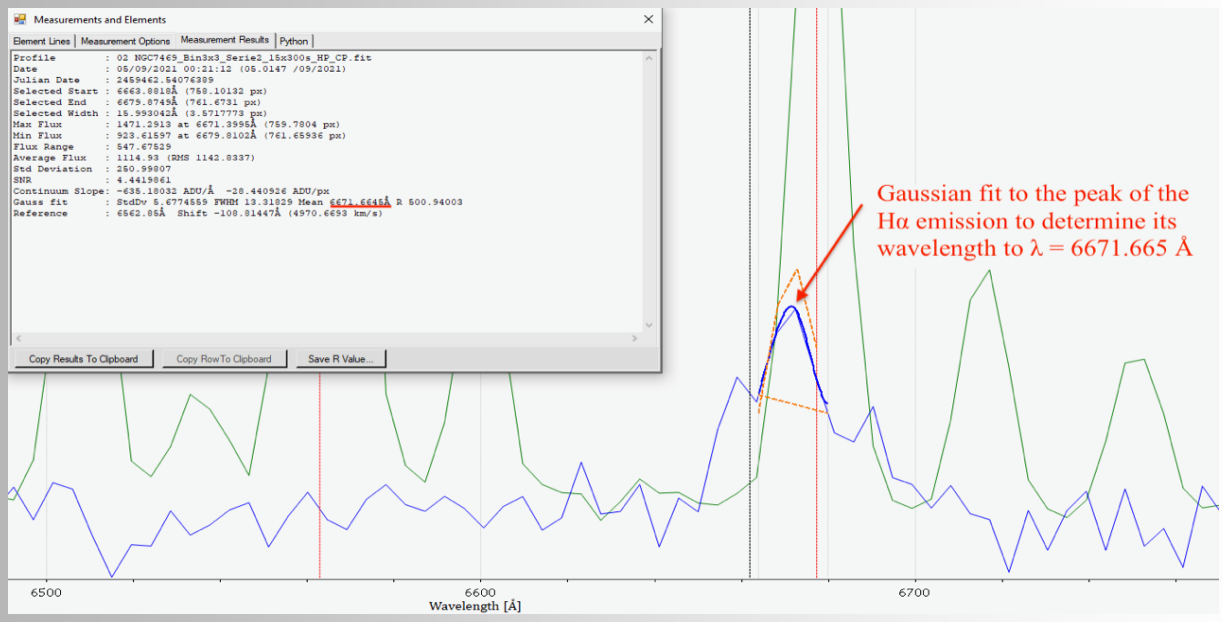


**Fig. 5:** Gaussian fit at Hα to determine the peak wavelength

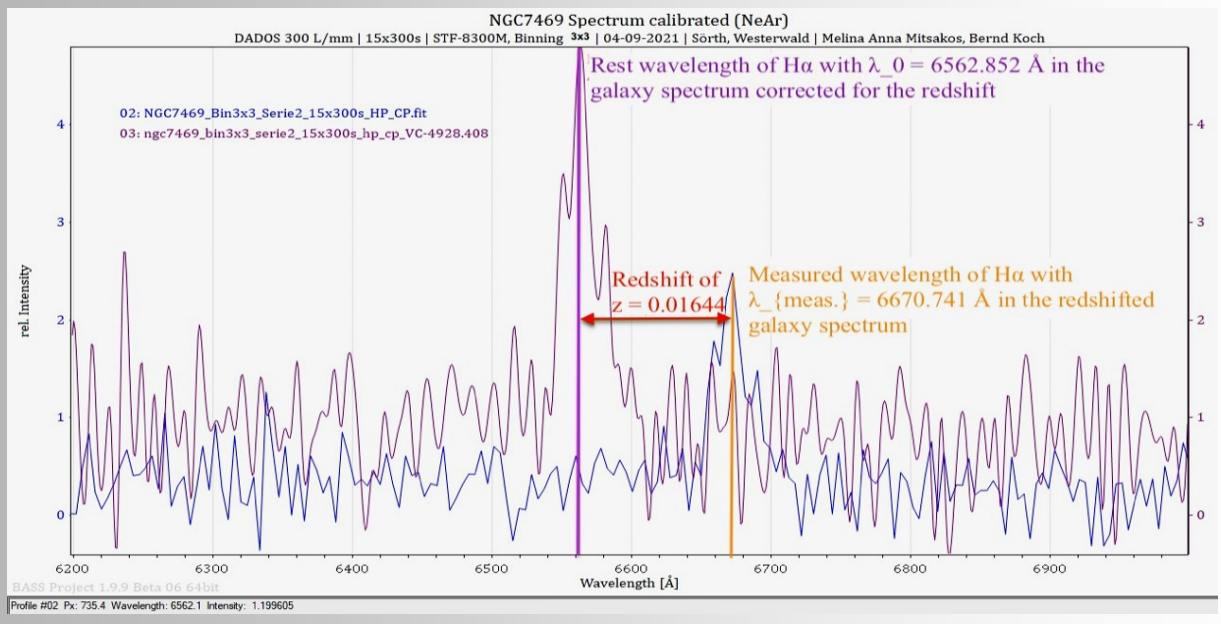


**Fig. 6**: Fully calibrated spectrum of NGC7469 (blue) and redshift corrected spectrum (purple)

Using the galaxy's measured redshift one can determine the non-relativistic (n.r.) radial velocity $v_r$ by applying the formula $v_{r\,(n.r.)} = cz$ which results in $v_{r\,(n.r.)} = 4928.4$ km/s with c being the velocity of light. Taking into account the relativity (r.) between galaxy and observer the formula changes to $v_{r(r.)} = (cz\text{^}2+2cz)/(z\text{^}2+2z+2)$, leading to a value of $v_{r(r.)} = 4887.9$ km/s. Although the relativistic radial velocity $v_{r(r.)}$ only has a fraction of 1.63% of the velocity of light c, the relativity seemingly influences the result.

One goal of this work was determining the Hubble Constant $H_t$ for the present (t = 0). Applying the general formula to my measurement of redshift leads to a result of $H_t = 0 = (v_{r(r.)})/(r(t = 0)) = (4887.9\text{ km/s})/(56.29\text{ Mpc}) = 86.84$ km/s/Mpc. However, the data concerning the distance of the galaxy contains quite a big standard deviation with $\sigma = 12.15$ Mpc. Hence, only the range in which the current Hubble constant lies can be narrowed down to $H_0 = 71.42$ km/s/Mpc –110.75 km/s/Mpc.

**Results and discussion**

The redshift of the galaxy NGC7469 could be determined on the basis of my spectra and measurements to z = 0. 01644. The SIMBAD database was first used to compare this value with other measurements. There, the redshift z is given as 0.016565, which corresponds to a deviation of -0.76% of my value from the SIMBAD value [4]. A comparison of my measurements with the NED (NASA Extragalactic Database), which states z = 0.01627 [1], shows a deviation of 1.04% (see Table 1).

| $z_{(measured)}$ | z NED | $\Delta(z)$ [%] | z SIMBAD | $\Delta(z)$ [%] | $H_{0\,(measured)}$ [km/s/Mpc] |
|---|---|---|---|---|---|
| 0.01644 | 0.01627 | 1.04 | 0.016565 | -0.76 | 71.42 –110.75 (~86.84) |

**Table 1:** Summary of the results of the redshift z and the Hubble Constant $H_0$; comparison between own measurements, the NED and SIMBAD

However, a more detailed look at of the values given in the databases shows that SIMBAD only references a single study, while the value of NED is an average of various studies over a longer period of time. Even though it must be taken into account, however, it must be taken into account that some values have apparently been roughly rounded, or that some values have been listed more than once, the average value of NED seems more relaible than the single value of SIMBAD.

It must also be noted that my measurement was only made on the Hα line and not on additional, emission lines whose z-values could have been averaged. This was due to the fact that other emission lines could hardly be seen and could therefore not be evaluated.

The value of the radial velocity is specified at NED with $v_r$ = 4877 km/s. The non-relativistic radial velocity $v_{r\,(n.r.)}$ = 4928.4 km/s calculated by me has a deviation of 1.05% from that value, while the relativistic radial velocity $v_{r\,(r.)}$ = 4887.9 km/s deviates by 0.22%. The measured redshift and thus the radial velocity of the galaxy are not only influenced by the expansion of space but also by the galaxy's own motion, e.g. due to gravitational effects. It occurs as relativistic Doppler effect in the spectrum. A look to the Internet did not provide information either on a known peculiar velocity of NGC 7469. Still, the expansion of space probably outweighs the relativistic Doppler effect in regard to the measured parameters because of the galaxy's large distance to us.

Depending on the conducted measurement of cosmological redshift, the range of the Hubble constant $H_0$ = 71.42 km/s/Mpc - 110.75 km/s/Mpc coincides with other findings. It has not been possible yet to determine a single value for the current Hubble Constant as two different methods (measurement of the cosmic microwave background or measurement of the redshift and distance of many objects) lead to varying results. The latter way of determining the Hubble constant is highly dependent on the precise measurement of distances to faraway objects, which turns out to be nontrivial as special events like supernovae of type Ia are needed. Especially for NGC 7469 the redshift-independent measurements of distance given at NED have a large standard deviation which causes the rather imprecise determination of the Hubble constant.

Further analysis of the galaxy spectrum was conducted regarding the velocity dispersion of the Hα emission line which is evoked by an expanding cloud of hydrogen in the galaxy's core around the active galactic nucleus. Consequently, the instrument dispersion was determined as well. These evaluations and results are presented in my original work which is to find in [5].

All measurements of the Hα emission, its redshift and velocity dispersion as well as instrument dispersion, means and standard deviations, and comparisons with observations by other investigators are shown on pages 30 & 31.

**References:**

[1] Data to NGC7469; http://ned.ipac.caltech.edu/
[2] JWST and HST observations of NGC7469; https://www.nasa.gov/image-feature/goddard/2022/hubble-peers-at-peculiar-pair-of-galaxies
[3] Calibration of the NeAr reference lamp; http://www.astrophoto.at/calibration-arne.html
[4] Data to NGC7469; https://simbad.u-strasbg.fr/simbad
[5] Projektarbeit (schuelerlabor-astronomie.de)

Measuring the redshift of galaxy NGC7469 to determine the Hubble constant

| | Average wavelength of the Gaussian fit on Hα [Å] | Measurement z [Wavelength of the Gaussian fit/ Wavelength Hα] - 1 | | Radial velocity v_r | Velocity dispersion of the reference spectrum at λ = 6677Å [Å in FWHM] | Velocity dispersion of the Hα line [Å in FWHM] (corrected by 9.1Å) | Velocity dispersion of the Hα line [km/s in FWHM] | Velocity dispersion of the Hα line [km/s in FWHM] (corrected by 9.1Å) |
|---|---|---|---|---|---|---|---|---|
| Overview | 6668.01 | 0.01602 | | Measurement v_r(r(n,r,)) [km/s]: c * Mean Measurement z | 9.30 | 21.10 | 2526.46 | 2517.36 |
| Wavelength of the Gaussian fit on Hα | 6668.58 | 0.01611 | | 4928.40 | 9.30 | 21.32 | 2465.60 | 2456.50 |
| Redshift z | 6668.70 | 0.01613 | | Measurement v_r(r(,)) [km/s]: (c^2*2+2cz)/(z^2+2z+2) with Mean Measurement z | 8.77 | 21.67 | 3074.38 | 3065.28 |
| Radial velocity v_r(r(n,r,)) = c * z (n,r, = non-relativistic) | 6668.81 | 0.01615 | | 4887.90 | 9.30 | 21.32 | 2435.15 | 2426.05 |
| Radial velocity v_r(r(,)) = (c^2*2+2cz)/(z^2+2z+2) (r, = relativistic) | 6670.01 | 0.01633 | | v_r [km/s]: c * z Simbad | 9.13 | 21.32 | 2465.60 | 2456.50 |
| Velocity dispersion of the Hα line [km/s] | 6670.03 | 0.01633 | | 4966.06 | 9.30 | 21.23 | 2465.57 | 2456.47 |
| Velocity dispersion of the Hα line [km/s in FWHM] | 6671.20 | 0.01651 | | v_r NED [km/s] | 9.48 | 21.32 | 2435.15 | 2426.05 |
| Resolving power of the spectrograph | 6671.20 | 0.01651 | | 4877.02 | 8.95 | 20.67 | 2617.80 | 2608.70 |
| Relation of Measurement v_(r(r,)) to c, c = 299792.458 km/s | 6671.40 | 0.01654 | | | 8.95 | 21.23 | 2496.02 | 2486.92 |
| Hubble constant H_0 | 6671.41 | 0.01654 | | Relative error: Measurement v_r(r(n,r,)) and v_r NED | 9.30 | 21.32 | 2465.60 | 2456.50 |
| | 6671.66 | 0.01658 | | 0.0105 | 9.12 | 21.23 | 2404.74 | 2395.64 |
| | 6671.67 | 0.01658 | | Relative error: Measurement v_r(r(,)) and v_r NED | Mean | Mean | Mean | Mean |
| | 6671.69 | 0.01658 | | 0.0022 | 9.17 | 21.25 | 2532.01 | 2522.91 |
| | 6671.72 | 0.01659 | | | Standard deviation | | Standard deviation | |
| | 6671.74 | 0.01659 | | Relation of Measurement v_(r(r,)) to c | 0.21 | | | 188.54 |
| | 6671.80 | 0.01660 | | 0.0163 | | | | |
| | 6671.84 | 0.01661 | | | Maximal intensity at λ = 6677Å | | | |
| | 6671.86 | 0.01661 | | r NED [Mpc] | 3891.86 | | | |
| | Mean: Mean wavelength of the Gaussian fits [Å] | Standard deviation: Mean wavelength of the Gaussian fits [Å] | Mean: Measurement z | 66.47 ± 4.67 | Minimal intensity 1 at the bottom of the peak at λ = 6677Å | Mean: Minimal intensity 1+2 | | |
| | 6670.74 | 1.34 | 0.01644 | 0.00020 | Hubble constant measurement [km/s/Mpc]: H_0 = (c * Measurement z)/r NED | 282.40 | 281.31 | |
| | Mean: Measurement z | Standard deviation: Measurement z | z Simbad | z NED | 69.28 - 79.75 (-74.14) | Minimal intensity 2 at the bottom of the peak at λ = 6677Å | Half maximum intensity at λ = 6677Å | |
| | 0.01644 | 0.00020 | 0.016565 | 0.01627 | | 280.21 | 1805.28 | |
| | Relative error: Mean Measurement z and z Simbad | Relative error: Mean Measurement z and z NED | | | | | | |
| | -0.00758 | 0.01041 | | | | | | |

Measuring the redshift of galaxy NGC7469 to determine the Hubble constant

| Velocity dispersion of the Hα line [km/s] | Comparison: my own results - reference of Cazzoli et al. 2020 | Correction of the FWHM value | Resolving power of the DADOS spectrograph, measured on the broadening of the line λ = 6677Å, FWHM |
|---|---|---|---|
| | | | 718 |
| 970.72 | Relative error:<br>Rounded mean Velocity dispersion [km/s] (own measurement) and Average velocity dispersion [km/s] (Cazzoli et al. 2020) | Measurement on the sharp line<br>λ = 6677Å | |
| 979.85 | -0.12 | 9.1±0.2Å | 718 |
| 961.58 | Relative error:<br>Rounded standard deviation [km/s] (own measurement) and Standard deviation of the average velocity dispersion [km/s] (Cazzoli et al. 2020) | ((23.1Å)^2-(9.1Å)^2)^(1/2) = 21.25±0.2Å | 762 |
| Mean:<br>Velocity dispersion of the Hα line [km/s] | -0.10 | | 718 |
| 970.72 | Relative error:<br>Velocity dispersion [km/s in FWHM] corrected by 9.1Å (own measurement) and Velocity dispersion [km/s in FWHM] (Cazzoli et al. 2020) | | 732 |
| Rounded mean:<br>Velocity dispersion of the Hα line [km/s] | -0.03 | | 718 |
| 971.00 | | | 704 |
| Standard deviation:<br>Velocity dispersion of the Hα line [km/s] | Resolving power R of the spectrograph (own measurement) | | 746 |
| 9.14 | 727.00 | | 746 |
| Rounded standard deviation:<br>Velocity dispersion of the Hα line [km/s] | Resolving power R of the spectrograph (simulation with Simspec) | | 718 |
| 9.00 | 593 | | 732 |
| Rounded: 971±9 km/s<br>The sides of the Hα line cannot be determined clearly because other emission lines contribute to the peak's profile and because the spectrograph has a certain imprecision regarding the width of the peaks. Hence, the FWHM value is used (measured in Ångström). It has a value of 21.25±0.2Å for Hα. | Resolving power R of the spectrograph (Cazzoli et al. 2020) | Mean:<br>Resolving power of the DADOS spectrograph | |
| Velocity dispersion of the Hα line corrected by 9.1Å [km/s in FWHM] | 20000 | | 727.33 |
| 2522.91 | | Rounded mean:<br>Resolving power of the DADOS spectrograph | 727.00 |
| References regarding the velocity and inner structure of NGC7469 (velocity with which the (hydrogen) gas rotates around the central black hole)<br>Reference of Cazzoli et al. 2020 (page 10) | | | |
| Average velocity dispersion of the Hα line [km/s] | | | |
| 1100 | | | |
| Standard deviation of the average velocity dispersion of the Hα line [km/s] | | | |
| 10 | | | |
| Velocity dispersion of the Hα line [km/s in FWHM] | | | |
| 2590 | | | |
| Reference of Peterson et al. 2004 and Bentz & Katz 2015:<br>Velocity dispersion of the Hα line [km/s in FWHM],<br>spectral resolution of ~9Å | Possible reasons for the deviation between the two references:<br>spectral resolution or variability of the galaxy's AGN<br>After adjusting the spectral resolution by Cazzoli et al., the result still showed a great deviation with 2100 km/s to 1615 km/s. Therefore the variability seems plausible. | | |
| 1615±119 | | | |

# Astronomy, Spectroscopy and Physics

Andreas Ulrich, Benediktbeuern (Germany)
andreas.ulrich@ph.tum.de

**Abstract**

Professional as well as amateur astronomy have made tremendous progress in the last decades. This article presents potential spectroscopic observations to be performed by amateurs. The focus is on observations outside of typical star spectroscopy. Several examples in this direction are discussed.

## Introduction

Both professional as well as amateur astronomy have made tremendous progress since I became interested in this field during my time at school in the 1960ies. The development of CCD cameras and computer technology is of course the main reason for this progress. Active and adaptive optics contributed greatly and improved the performance of professional telescopes. Automated telescopes on the ground and in space provide a huge amount of data for the detection of transient phenomena and the compilation of surveys.

Improvement of the instrumentation for astronomy amateurs allows to reproduce many of the professional observations and to contribute to scientific programs. As a physicist I was also interested in planning my own observations. Spectroscopic observations were always of particular interest for me since they are closely related to phenomena in physics. There is a sub-community of astronomy amateurs capable of performing advanced spectroscopic observations. With this article I want to motivate more amateurs to include spectroscopy in their observations. Professionally, I worked mainly with spectroscopy in the vacuum ultraviolet wavelength region ($\lambda$<180nm). Only at the end of my professional time this work was related to astronomy in the context of liquid noble gas scintillation detectors for direct dark matter search. I had very little time for observations I consider interesting. Now, after my retirement I got a teaching call from the Hochschule Landshut, Germany. An observatory is being set up at this institution for teaching purposes. In this context I have put together a list of potential observations which students could try to make during lab courses in physics. Some spectroscopic observations from this list I want to share with readers from the amateur community.

Below I list and briefly discuss potential observations and mention what could be learned for physics where it is possible. Most of the examples I have not yet tested and I would be interested in getting some response e.g. by publications in this journal presenting the results. Most observations should not require sophisticated instrumentation since they deal with rather bright objects.

**Suggested observations**

In the following I list some ideas for spectroscopic measurements which are in some sense related to astronomy. Since the atmosphere is always between us and the astronomic objects I start with observations from the field of atmospheric optics. Light scattering and absorption play an important role in this context. Then I discuss effects to be observed for bright objects like the sun and the moon.

**The Atmosphere**

A first step for spectroscopy in the sky is to record a spectrum of the blue sky and the sun. The sunlight has of course to be attenuated in such a way that it can be compared with the spectrum of the sky close to the sun. I have made this measurement with high school students and one can learn about Rayleigh scattering from the results. A ratio of the two spectra shows nicely the $\lambda^{-4}$ dependence of Rayleigh scattering. I would find it interesting to study the spectrum of the blue sky more systematically. How does it change with the distance from the sun? How does it look at the time of sunset or sunrise? How is it related to weather conditions? I am sure that all this is known in detail in a field called atmospheric optics. With the discussion of climate-change it could be interesting to take a closer look at the atmosphere at different places and time and perform long term studies. Spectra of clouds must tell something about light scattering. In spring this year (2022) we had in Bavaria, Germany a lot of sand from the Sahara in the atmosphere changing the color of the sky significantly. I also find it interesting if the telluric lines of water and oxygen (Fraunhofer A to C) correlate in their intensity ratio with humidity in the air when using the sun or the moon as the light source. One could also look for spectra of rainbows, lightning strokes, and try to record spectra of meteors/meteorites.

When I took a trip to Norway in winter I missed to take a spectrometer with me. Spectroscopy of polar light could be interesting. Having worked for a while on the calibration of the Pierre Auger cosmic ray detector where the C to B Transitions of molecular nitrogen between 300 and 400nm play the dominant role I was wondering if these lines appear also in the polar light. Spectra I found on the internet stopped at 400nm. I am also wondering if emission related to polar light can be observed at any place and time in spectra recorded with long exposure times of the dark sky because of the permanent flux of cosmic rays. Airglow may also contribute.

Another atmospheric phenomenon at an altitude of about 100 km is the so-called sodium-flash. I had learned about this effect from Dr. Peter Schlatter, Switzerland. We have made an observation together on the campus of the observatory Haute Provance, southern France and published our data in Spectrum Nr. 47, 1/2014, page 8. Shortly after sunset the sunlight illuminates a layer of sodium atoms. Resonant fluorescence induced by the remaining intensity in the sodium D line from the sun overcomes the dip in the spectrum in the scattered light and the

D line develops from an "absorption" line into an emission line. This effect demonstrates the idea of the guide stars without using a ground-based laser to induce fluorescent light.

**The Sun**

An easy way to study the spectrum of the sun, space-resolved on the sun's surface is to use a small telescope, project the sun on a screen and place an optical fiber or the entrance slit of a spectrometer in the middle of this screen. I have put absorption in quotation marks above, because Fraunhofer lines like the sodium D line are only a measure how deep one can look into the solar plasma and this depends on the wavelength dependent absorption coefficient. For geometrical reasons one should also look deeper into the solar plasma in the center of the sun than on its rim. I looked for this effect and recorded spectra by letting the sun move across an optical fiber connected to a spectrometer. Spectra recorded on the rim and the center are shown in Fig. 1. Since the plasma is hotter when looking deeper inside (optical depth: absorption coefficient times geometrical distance), the spectrum at the rim is redshifted with respect to the spectrum recorded in the sun's center.

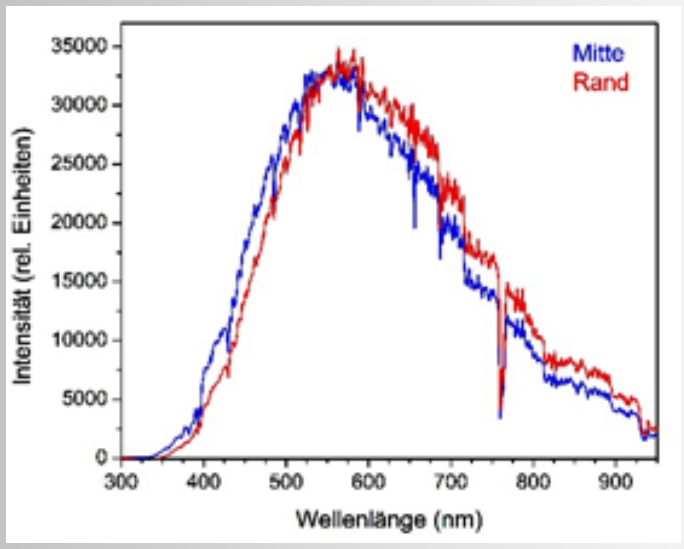


**Fig. 1:** Spectra recorded in the center (Mitte) and the rim (Rand) of the sun. Intensity (Intensität) versus wavelength (Wellenlänge). The redshift of the spectrum at the rim is explained in the text.

Comparing spectra inside and outside of sunspots would also be interesting. Following spectra of the sun during partial or total eclipses of the sun could be another technically simple observation providing interesting data. Also: maybe one can observe the corona spectroscopically without an eclipse by looking very closely at the rim of the sun?

**The Moon**

Spectra of the moonlight contain of course information about the material on the surface of the moon. I had learned that rocks differ in their reflectivity mainly in the infrared. Studies of moonlight from various places on the moon were for example used to prepare spaceflight missions to the moon. Color-enhanced photographs of the moon show a colorful picture. To perform a different measurement I decided to compare spectra of the sun and the full moon averaging over the surface of both celestial objects. I performed such measurements from the Emberger Alm, Austria, during the time of full moon and at a time when the sun and the moon culminated at essentially the same altitude. The result is published in [1] and also shows a color picture of the moon. A measurement using the moon as on optical screen would be an observation of the spectrum of the moonlight during a partial or total eclipse of the moon. During that time the light from the moon will contain information of the earth's atmosphere. Does e.g. the sodium D line now become significantly deeper due to absorption in the sodium layer around the earth? It should. A speculation is the question if it would be possible to measure the spectra of moon blinks when meteorites hit the surface of the moon. This should show some emission lines. I only mention this because one can keep in mind that modern spectrometers and their software allow to automatically record spectra within short time intervals and store them for later analysis. Thereby, spectroscopy can also be performed for transient events.

**The Planets**

Similar to spectroscopy of moonlight the spectra of planets will show a composition of sunlight and effects of their surface and atmosphere where it exists. Spectroscopic observations I could also consider would be, to follow occultations of planets by the moon or stars by planets. Spectra of comets might also be interesting.

**The Stars**

Spectroscopic measurements of stars are nowadays routinely performed, also by amateur astronomers. In this field the studies merge with professional astronomy and are outside the scope of this article which tries to motivate simple observations performed out of curiosity and interest in physics processes.

**Conclusion**

Adding the option of spectroscopic measurements to astronomical observations can open a way to obtain interesting results related to basic-physics effects like emission, absorption, scattering of light and fluorescence.

**Reference**

[1] Andreas Ulrich, "Sterne und Weltraum" February 2011, p. 74

## AAVSO Selects Dr. Brian Kloppenborg as Executive Director

The American Association of Variable Star Observers (AAVSO) is excited to welcome Dr. Brian Kloppenborg as the new Executive Director. "Brian brings the skills needed to advance AAVSO's scientific impact, combined with experience in management and project budgeting," notes AAVSO President David Cowall.

Prior to AAVSO, Brian was a research scientist at Georgia Tech Research Institute, serving as a subject matter expert, lead engineer, product owner, and project director on over $120M of sponsored programs.

Founded in 1911, AAVSO is an international organization enabling individuals to contribute to research on stars that vary in brightness or spectra. AAVSO has had 6,000+ star observers worldwide to date. Currently, these volunteers collectively report about 13,000 observations *every night* in support of professional astronomers.

Dr. Kloppenborg holds a Ph.D. in Physics, with an Astrophysics specialty, from the University of Denver. His research interests span photometry, spectroscopy, astrometry, and long-baseline optical interferometry of eclipsing binaries, novae, and young stellar objects. His work has been published in *Nature*, *ApJ*, *JAAVSO*, and other scholarly journals. Brian also ran a small business providing data science, machine learning, and GPU accelerated computing services.

To learn more about AAVSO, visit us at www.aavso.org.